The Journal of Chemical Physics

RESEARCH ARTICLE | APRIL 25 2024

Ultrafast electron diffraction of photoexcited gas-phase cyclobutanone predicted by *ab initio* multiple cloning simulations

Special Collection: Prediction Challenge: Cyclobutanone Photochemistry

Dmitry V. Makhov ; Lewis Hutton ; Adam Kirrander ; Dmitrii V. Shalashilin

J. Chem. Phys. 160, 164310 (2024)
https://doi.org/10.1063/5.0203683

AIP Publishing

The Journal of Chemical Physics ARTICLE pubs.aip.org/aip/jcp

Ultrafast electron diffraction of photoexcited gas-phase cyclobutanone predicted by *ab initio* multiple cloning simulations

Cite as: J. Chem. Phys. 160, 164310 (2024); doi: 10.1063/5.0203683
Submitted: 15 February 2024 • Accepted: 2 April 2024 •
Published Online: 25 April 2024

Dmitry V. Makhov,[1,2,a)] Lewis Hutton,[3] Adam Kirrander,[3] and Dmitrii V. Shalashilin[1]

AFFILIATIONS

[1] School of Chemistry, University of Leeds, Leeds LS2 9JT, United Kingdom
[2] School of Mathematics, University of Bristol, Fry Building, Woodland Road, Bristol BS8 1UG, United Kingdom
[3] Physical and Theoretical Chemistry Laboratory, Department of Chemistry, University of Oxford, Oxford OX1 3QZ, United Kingdom

Note: This paper is part of the JCP Special Topic on Prediction Challenge: Cyclobutanone Photochemistry.
[a)] **Author to whom correspondence should be addressed:** d.makhov@leeds.ac.uk

ABSTRACT

We present the result of our calculations of ultrafast electron diffraction (UED) for cyclobutanone excited into the S_2 electronic state, which is based on the non-adiabatic dynamics simulations with the *Ab Initio* Multiple Cloning (AIMC) method with the electronic structure calculated at the SA(3)-CASSCF(12,12)/aug-cc-pVDZ level of theory. The key features in the UED pattern were identified, which can be used to distinguish between the reaction pathways observed in the AIMC dynamics, although there is a significant overlap between representative signals due to the structural similarity of the products. The calculated UED pattern can be compared with the experiment.

I. INTRODUCTION

Ultrafast electron diffraction (UED) has evolved into a powerful method for structural dynamics.[1,2] Although UED and the closely related method of ultrafast x-ray scattering[3,4] arguably provide the most direct access to structural dynamics in photoexcited molecules, the interpretation of experiments is nontrivial. Despite significant progress in the development of inverse methods, which aim to produce a (time-dependent) molecular model commensurate with the experimental data,[5–9] the gold standard for interpreting ultrafast experiments remains the comparison to high-quality simulations of the photoexcited target molecule. However, such simulations are challenging, and their veracity depends keenly on numerous methodological choices. As a much needed step toward surveying and evaluating good practice, the Journal of Chemical Physics recently announced the *Prediction Challenge: Cyclobutanone Photochemistry,* to which this paper is a response.

There have been a number of different methods put forth under the collective term of nonadiabatic dynamic methods. Methods can broadly be partitioned into grid-based and on-the-fly methods. Grid-based methods, such as multiconfigurational time-dependent Hartree (MCTDH) and its multilayer variant (ML-MCTDH), are capable of giving high-accuracy results but at the cost of expensive precomputed potential energy surfaces (PESs).[10,11] To alleviate this need, on-the-fly trajectory-based methods are often employed, ranging from trajectory surface hopping (TSH), where nuclei are treated classically and electronic quantities are calculated from electronic structure methods, nonadiabatic events are then simulated with hopping events between electronic states.[12] To increase the quantum nature of the nuclei, full multiple spawning (FMS) or *ab initio* multiple spawning (AIMS) can be used. FMS/AIMS uses a series of Gaussian basis functions to recreate a nuclear wavepacket; each of these Gaussians is propagated classically by their centroid position, with spawning events happening between surfaces in areas of configuration space with high nonadiabatic coupling.[13–16] Another technique using classically guided Gaussians is multiconfigurational Ehrenfest (MCE). More details on MCE with cloning, which is known

as *Ab Initio* Multiple Cloning (AIMC), can be found in Sec. II. However, briefly, multiple Gaussians are propagated according to Ehrenfest forces, and a cloning algorithm is employed in a similar way to spawning in AIMS.[17,18] For a more detailed summary of the methods available, see Ref. 19. With such a large number of possible methods, questions naturally arise about the accuracy of these methods when calculating experimental observables.

Cyclobutanone [$(CH_2)_3CO$] is a small cyclic ketone shown both experimentally and theoretically to have a rich photochemistry.[19–25] After cyclobutanone is excited into its S_1 ($n\pi^*$) state, both C_3H_6/CO and C_2H_4/CH_2CO are produced in a 2:3 ratio although this ratio has been shown to be strongly wavelength dependent.[23] Further studies into the photodynamics of cyclobutanone after excitation into S_1 found an α ring-opening reaction to be the dominant deactivation pathway and can result in the formation of ketene (CH_2CO). It should be noted that this study takes place in a solvent environment.[26] These reaction pathways have also been observed from static calculations and AIMS simulations.[27,28] In addition, the role of triplet states is expected to be minimal unless the excitation energy is low enough.[26] The second absorption band arises from an n-3s Rydberg transition (S_2).[29–31] Studies probing the dynamics initiated from the S_2 state using time-resolved mass spectrometry and time-resolved photoelectron spectroscopy indicate that an out-of-plane ring puckering motion is present, allowing for the rapid S_2/S_1 decay.[32] This mechanism was supported by a five-dimensional linear vibronic Hamiltonian used for MCTDH simulations.[33] It has been suggested that after decay to the S_1 state, the deactivation mechanism of cyclobutanone should be ultrafast, producing a product of m/z = 42.[32]

The challenge is motivated by an experiment at the SLAC Megaelectronvolt ultrafast electron diffraction (SLAC MeV-UED) facility, where a gas-phase sample of cyclobutanone is irradiated with a 200 nm laser pulse and time-resolved UED signals are recorded. At this excitation energy, a low-lying n → 3 s (S_2) Rydberg state in cyclobutanone is excited.[29–32]

In this work, the photodynamics of cyclobutanone is simulated using the *Ab Initio* Multiple Cloning (AIMC)[34–36] approach, which is, in principle, a fully quantum, formally exact methodology based on using Gaussian coherent states propagated by Ehrenfest trajectories as a basis for the quantum dynamics of nuclear wave functions. AIMC was successfully applied before[37–41] to simulate the process of the photodissociation of a number of heterocyclic molecules. Based on AIMC dynamics results, the isotropic gas phase time-resolved UED pattern of cyclobutanone photoexcited using a 200 nm pulse is calculated for the initial 200 fs of dynamics, allowing for direct comparison to experimental data.

II. THEORETICAL METHODS

A. AIMC

As the AIMC methodology was extensively described before,[34–37] here we provide only a summary of the technique. The AIMC method represents the further development of the Multi Configurational Ehrenfest (MCE)[43–46] approach and makes use of the following wavefunction ansatz:

$$|\Psi(\mathbf{R},\mathbf{r},t)\rangle = \sum_n c_n(t)|\chi(\mathbf{R},t)\rangle \sum_I a_I^{(n)}|\phi_I(\mathbf{r};\mathbf{R})\rangle, \quad (1)$$

where $\mathbf{R}$ and $\mathbf{r}$ are the electronic and nuclear coordinates, respectively. The electronic part of each basis function is represented in a basis of adiabatic electronic states $|\phi_I\rangle$, and the nuclear part is a moving Gaussian coherent state,

$$|\chi_n(\mathbf{R},t)\rangle = \left(\frac{2\alpha}{\pi}\right)^{\frac{N_{\mathrm{dof}}}{4}} \times \exp\left(-\alpha(\mathbf{R}-\mathbf{R}_n)^2 + \frac{i}{\hbar}\mathbf{P}_n(\mathbf{R}-\mathbf{R}_n) + \frac{i}{\hbar}\gamma_n(t)\right), \quad (2)$$

which is a Gaussian-shaped de Broglie wave centered at $\mathbf{R}_n$ with momentum $\mathbf{P}_n$ and phase γ_n. The motion of Gaussians $|\chi_n\rangle$ is guided by the Ehrenfest force,

$$\dot{\mathbf{R}}_n = M^{(-1)}\mathbf{P}_n,$$

$$\dot{\mathbf{P}}_n = -\sum_I \left|a_I^{(n)}\right|^2 \nabla V_I^{(n)} + \sum_{I\neq J} a_I^{(n)*} a_J^{(n)} \mathbf{d}_{IJ}^{(n)} \cdot \dot{\mathbf{R}}_n \left(V_I^{(n)} - V_J^{(n)}\right), \quad (3)$$

where V_I is the potential energy surface of the Ith electronic state, $\mathbf{d}_{IJ}$ is a non-adiabatic coupling vector, and M is a diagonal matrix of atomic masses. As the force depends on Ehrenfest amplitudes $a_I^{(n)}$, the equations of motion (3) must be solved simultaneously with the equations for $a_I^{(n)}$,

$$\dot{a}_I^{(n)} = -\frac{i}{\hbar} V_I^{(n)} a_I^{(n)} - \sum_J \dot{\mathbf{R}}_n \cdot \mathbf{d}_{IJ} a_J^{(n)}, \quad (4)$$

where the right-hand side is the electronic Hamiltonian for the nth basis function. Finally, phase γ_n is propagated semiclassically as $\dot{\gamma}_n = \mathbf{P}_n\dot{\mathbf{R}}_n/2$.

It is well known that Ehrenfest trajectories misguide basis sets when several non-interacting electronic states have significant amplitudes. The cloning procedure is applied in the AIMC approach in order to address this issue. In principle, cloning can be viewed as a straightforward way of spawning employed in the multiple spawning method.[19] The idea of cloning is to replace a basis function with two clones, each of which is guided, in most cases, by just one potential energy surface. In the simplest case of two electronic states,

$$c_n|\chi_n\rangle\left(a_1^{(n)}|\phi_1\rangle + a_2^{(n)}|\phi_2\rangle\right) = c_n'|\chi_n\rangle\left(0\times|\phi_1\rangle + \frac{a_2^{(n)}}{|a_2^{(n)}|}|\phi_2\rangle\right) + c_n''|\chi_n\rangle\left(\frac{a_1^{(n)}}{|a_1^{(n)}|}|\phi_1\rangle + 0\times|\phi_2\rangle\right), \quad (5)$$

where

$$c_n' = c_n|a_2^{(n)}|; c_n'' = c_n|a_1^{(n)}|. \quad (6)$$

The total contribution of two clones into the wave function $|\Psi(\mathbf{R},\mathbf{r},t)\rangle$ is exactly the same as that of the original basis function. However, cloning increases the size of the basis set, creating additional flexibility as two clones can now move in different directions. The cloning is applied when the magnitude of the breaking force $\mathbf{F}_I^{(br)} = |a_I|^2\left(\nabla V_I - \sum_J |a_J|^2 \nabla V_J\right)$ exceeds a threshold, and, at the same time, the magnitude of non-adiabatic coupling is below

a second threshold. Cloning is an extremely important part of the AIMC method, as it allows AIMC to reproduce the bifurcation of the wave function at conical intersections.

The trajectories in the AIMC approach can be calculated independently using potential energy forces and non-adiabatic coupling vectors calculated "on the fly" by an electronic structure code. Then, the time-depended Schrödinger equation for amplitudes c_n is solved in post-processing on the precalculated trajectory-guided basis (1).

In practice, to achieve good convergence, a number of sampling techniques have to be used. Swarms of coupled trajectory guided Gaussians, as well as their trains guided by the same trajectories, are among those techniques.[44] It has been demonstrated that MCE can produce results that are well converged,[45] and AIMC, its *ab initio* direct dynamics version, is more accurate than surface hopping or Ehrenfest dynamics.[46,47] A technique that allows for taking into account the pulse shape and dynamics that occur during the excitation has been developed.[48] In its simplest form, which is used in the present paper, AIMC can yield a qualitative or semiquantitative picture of the process, similar to that given by surface hoping, AIMS,[19] and many other popular techniques.

B. Ultrafast electron diffraction

For the modeling of the UED signals, we anticipate that the experimental data in this challenge can be modeled reliably using the independent atom model (IAM). This approximates the scattering signal as a coherent sum of scattering from isolated atoms centered at the positions of the nuclei in the target molecule. Notably, this model excludes the contribution of the bonding electrons and the characteristics of the electronic states of the molecule. Should the quality of the experimental data necessitate that these effects are accounted for, then numerical codes capable of this exist,[49–52] albeit at significantly higher computational costs.

The total (energy-integrated) scattering cross section into the solid angle $d\Omega$ at time t is given by[53–55]

$$\frac{d\sigma}{d\Omega}\Big/\left(\frac{d\sigma}{d\Omega}\right)_{\mathrm{Rh}} = I_{\mathrm{tot}}(\mathbf{s},t), \tag{7}$$

where $\mathbf{s} = \mathbf{k}_0 - \mathbf{k}_1$ is the scattering vector expressed in terms of the wave vectors of the incoming and outgoing electrons. The scattering is given in units of the Rutherford cross section $(d\sigma/d\Omega)_{\mathrm{Rh}}$, which includes the s^{-4} scaling factor.[56,57] Note that the expression above does not account for the duration of the electron pulse, which may be included via a temporal convolution of the predicted signal.

General expressions that account for the full wavefunction in Eq. (1), including the non-local nature of the individual Gaussian coherent states, have been derived previously.[53] Given the sparse basis used in the present simulations, we resort here to the diagonal bracket-averaged Taylor (BAT) expansion approximation[53] and assume that expansion coefficients are independent of time, $c_n \approx c_n(t)$, giving the total scattering intensity as follows:

$$I_{\mathrm{tot}}(\mathbf{s},t) = \sum_{n=1} |c_n|^2 I_n(\mathbf{s},\mathbf{R}_n(t)). \tag{8}$$

In this simplified form, sufficient for our present needs, the scattering from each trajectory is given by IAM as follows:[58]

$$I_n(\mathbf{s},\mathbf{R}_n(t)) = |F(\mathbf{s},\mathbf{R}_n(t))|^2 + S_{\mathrm{inel}}(s), \tag{9}$$

where $S_{\mathrm{inel}}(s)$ is the inelastic scattering, which is independent of molecular geometry and isotropic, as underscored by its dependence only on the amplitude of the momentum transfer vector, $s = |\mathbf{s}|$. It is given by an incoherent summation of the individual atomic contributions,

$$S_{\mathrm{inel}}(s) = \sum_{A=1}^{N_{\mathrm{at}}} S_A(s), \tag{10}$$

with N_{at} being the number of atoms in the molecule. The corresponding elastic contribution is given by the form factor $F(\mathbf{s},\mathbf{R}_n(t))$,

$$F(\mathbf{s},\mathbf{R}_n(t)) = \sum_{A=1}^{N_{\mathrm{at}}} f_A^e(s) e^{i\mathbf{s}\mathbf{R}_{nA}(t)}, \tag{11}$$

where $f_A^{\mathrm{e}}(s)$ are the atomic form factors and $\mathbf{R}_{nA}(t)$ is the position vector for atom A in trajectory n. The form factors for electron scattering are $f_A^{\mathrm{e}} = (f_A^{\mathrm{x}} - Z_A)$, where f_A^{x} is the x-ray scattering form factor and Z_A is the atomic number.[56,57] Both $f_A^{\mathrm{x}}(s)$ and $S_A(s)$ are tabulated.[59] For high energy electron scattering, it is sometimes necessary to use form factors with relativistic corrections,[60,61] but this is not done presently.

When the target is a gas of anisotropic molecules, $|F(\mathbf{s},\mathbf{R}_n(t))|^2$ in Eq. (9) is replaced by its rotationally averaged counterpart, $\langle|F(s,\mathbf{R}_n(t))|^2\rangle$,[62]

$$\langle|F(s,\mathbf{R}_n(t))|^2\rangle = \sum_{A,B}^{N_{\mathrm{at}}} f_A^{\mathrm{e}}(s) f_B^{\mathrm{e}}(s) \frac{\sin(sR_{nAB}(t))}{sR_{nAB}(t)}, \tag{12}$$

where $R_{nAB}(t) = |\mathbf{R}_{nA}(t) - \mathbf{R}_{nB}(t)|$ is the distance between atoms A and B in trajectory n.

III. COMPUTATIONAL DETAILS

The trajectories were calculated using our own AIMC code, where potential energies, forces, and non-adiabatic couplings were given "on the fly" by the MOLPRO[63] electronic structure package at the SA(3)-CASSCF(12,12)/aug-cc-pVDZ level of theory. We note that the electronic structure method has been benchmarked in another paper submitted to the same challenge by one of the co-authors (AK). In brief, three electronic states were taken into consideration: a ground state and two lowest singlet excited states. Higher energy Rydberg states have been shown to exist (3p character) but are unlikely to be important for dynamics after excitation into S_2; therefore, we do not include them in our simulations.[33] We also do not take triplet states into consideration in this work, as they have been shown to only play a role in dynamics upon excitation with long wavelengths.[26] The initial positions and momenta for all trajectories are randomly sampled from the ground state vibrational Wigner distribution using vibrational frequencies and normal modes calculated at the same level of theory. This ground state wavepacket is then simply lifted to the second excited state within the Condon approximation. As in our previous simulations,[34,37–41] the cloning thresholds were taken as 5×10^{-6} a.u. and 2×10^{-3}

a.u. for the magnitude of breaking force and non-adiabatic coupling, respectively. In order to prevent uncontrolled growth of the number of branches, a maximum of three cloning events per trajectory are allowed.

In *ab initio* dynamics, the number of trajectories is severely limited by the high cost of electronic structure calculations (especially for larger molecules). When the initial multi-dimensional wavefunction is randomly sampled with a small number of Gaussians, these Gaussians, due to the high dimensionality of the system, will be located far away from each other with no coupling between them. Applying constraints to run Gaussians closer together would be an inefficient use of computer time unless we need to reproduce a particular quantum effect of the nuclear motion. In this work, we use a simplified semiclassical version of AIMC, where we do not consider the coupling between the trajectories. Instead, each branch simply gets its amplitudes at the time of cloning, and this amplitude determines the statistical weight of that branch.

We initially run an ensemble of 39 Ehrenfest trajectories with the number of branches growing in the process of cloning. All trajectories were propagated for ~200 fs with a 0.06 fs (2.5 a.u.) timestep. The relatively small number of trajectories and short duration of the dynamics are due to the strict deadline for this work. Nevertheless, despite not very good statistics, our calculations show clear UED patterns for the cyclobutanone photodynamics.

IV. RESULTS AND DISCUSSION

A. Dynamics

Figure 1 presents the dynamics of the populations for S_0, S_1, and S_2 electronic states. For the first 25 fs of dynamics, the molecules stay in the S_2 state, and then $S_2 \rightarrow S_1$ population transfer starts. The growing population of the S_1 state immediately initiates the next step of population transfer, from S_1 into the ground state. Within the next 10 fs, the S_1 state population reaches the equilibrium level of about 20%, when the rates of $S_2 \rightarrow S_1$ and $S_1 \rightarrow S_0$ transfers are about the same. For the rest of our dynamics, the S_1 state population is fluctuating around this level, while the S_2 state exhibits exponential decay into the ground state $S_2 \rightarrow S_1 \rightarrow S_0$.

The transfer of population between electronic states initiates the process of cloning, which starts at about 50 fs in time and continues uniformly for the duration of the dynamics. By 200 fs, cloning gives rise to 121 branches from the initial 39 trajectories. The small number of initial conditions limits the sampling of the phase-space in the current simulations and is unlikely to result in fully converged calculations. This aspect will be further considered and evaluated in the planned subsequent work.

Figure 2 shows the dynamics of C–C bonds breaking in the cyclobutanone ring. The bond is considered broken when the distance between two atoms exceeds 3 Å. The process of ring opening starts at about 25 fs, simultaneously with the beginning of the non-adiabatic decay of the S_2 state by breaking β-CC bonds. The analysis of trajectories shows that the length of one of β-CC bonds in the molecule often increases toward dissociation from the very beginning of the dynamics, while the lengths of other CC bonds oscillate with a period of about 20–30 fs. Within the next 50 fs, 30% of β-CC bonds break, which corresponds to 60% of the opened rings. At this stage of the dynamics, α-CC bonds are starting to break. In the vast majority of cases, α-CC bonds break in already opened rings, creating ethylene $(CH_2)(CH_2)$ and ethenone $(CO)(CH_2)$ molecules. In some of these ethenone molecules, C=C bonds also later break, creating CO and CH_2 radicals.

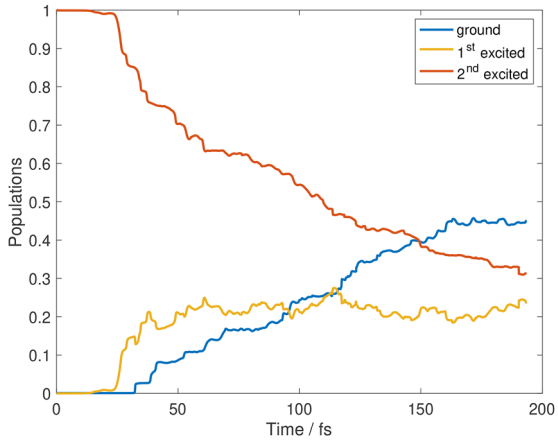

FIG. 1. Dynamics of S_2 (red), S_1 (yellow), and S_0 (blue) electronic state populations for the cyclobutanone molecule after its photoexcitation into the S_2 state.

After about 100 fs, some opened rings are beginning to close again (or, at least, their ends approach each other to less than 3 Å). Later, the ring can open again, creating an oscillatory behavior in the number of broken bonds.

By the end of the dynamics, the yield in the $(CH_2)(CH_2)$ + $(CO)(CH_2)$ dissociation channel is 40.6%, the yield in the $(CH_2)(CH_2)$ + (CO) + (CH_2) dissociation channel is 3.5%, and the yield of ring opening is 31.0%; also, 17.2% of molecules have remained in the closed ring form. The remaining 7.7% are found

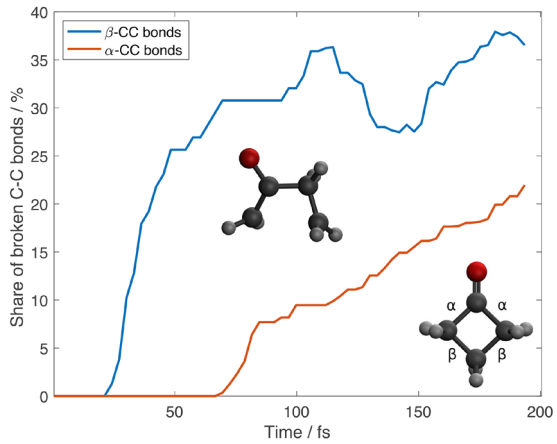

FIG. 2. Share of broken α- (red) and β- (blue) CC bonds as a function of time for the cyclobutanone molecule after its photoexcitation into the S_2 state. In most cases, the breaking of an α-bond is preceded by the breaking of the opposite β-bond in the same ring. Two structures are displayed as insets; the bottom right structure shows the definition of α- and β-CC bonds, while the center structure is an optimized minimum energy conical intersection optimized using SA(3)-CASSCF(12,12)/aug-cc-pVDZ.

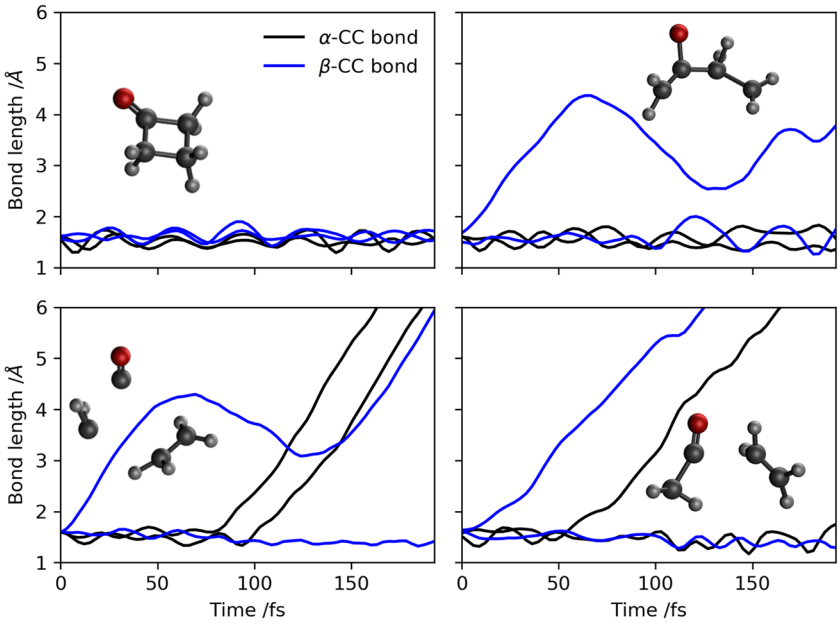

FIG. 3. All carbon–carbon bond lengths for the four-membered ring are plotted as a function of time for an exemplary trajectory in each of the four reaction outcomes. Panel (a) shows unreactive trajectories that stay in the Franck–Condon geometry, (b) displays the β ring opening, (c) shows the formation of C_2H_4 and CH_2CO and finally (d) shows where CO, CH_2, and C_2H_4 are produced. Representative structures for each reaction pathway, taken at arbitrary times in the simulations, are shown as insets in each panel.

at various other intermediate configurations at the end of our 200 fs dynamics; the longer-term dynamics will be a subject of our future work.

To aid our understanding of individual reaction pathways, Fig. 3 shows the bond lengths of the carbon backbone as a function of time for each reaction pathway discussed above; this yields four distinct pathways. Figure 3(a) shows no reaction taking place; all bonds stay sub 2 Å, indicating cyclobutanone remains in the Franck–Condon geometry for the duration of our simulations. There is still the potential for reactions to happen at longer time scales than have been simulated. Panel (b) shows a single bond breaking in the β position of the four-membered ring in a ring-opening reaction. Here, there is an immediate increase in the bond length of a β-CC bond in the S_2 state, confirming what is observed in Fig. 2. A maximum distance of ~4.5 Å is reached where velocities are reversed, reducing the bond distance to a minimum of ~3 Å. It is noteworthy that very few simulations underwent an α-CC ring opening process, in contrast to what has been previously observed as the dominant reaction pathway.[26] We have, therefore, optimized a minimum energy conical intersection (MECI) using SA(3)-CASSCF(12,12)/aug-cc-pVDZ, shown in the center inset in Fig. 2 displaying the β-CC ring opening. The main reaction pathway observed in our simulations is displayed in Fig. 3(c), with an initial β-CC ring opening reaction observed, followed by a subsequent break of an α-CC bond to yield CH_2CO and C_2H_4 in a stepwise mechanism. From our simulations, we see that this process always takes place in the order of β-CC bond breaking, likely decaying via the MECI shown in Fig. 2, then α-CC bond breaking, which is linked to the S_1/S_0 MECI shown in Ref. 28. Further fragmentation is possible with CH_2CO being able to fragment to produce CO and a CH_2 radical; however, this appears to be a minor channel in our simulations. The trajectory shown in Fig. 3(d) also displays the "tethered" motion shown in Fig. 3(b), causing a rebound effect observed in panel (d) until the full dissociation event has taken place.

B. Ultrafast electron diffraction

The AIMC simulations presented in Sec. IV A serve as a framework to calculate the total rotationally averaged UED pattern for

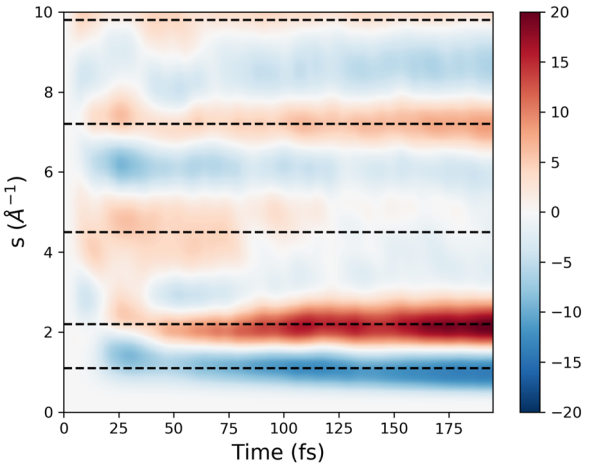

FIG. 4. Gas-phase UED pattern, $\%I_{tot}(s,t)$ in Eq. (13), for cyclobutanone calculated using the IAM with all trajectories and branches from our dynamics simulations. Five key features in the UED pattern are highlighted with horizontal dashed lines.

cyclobutanone using the methodology presented in Sec. II B. The UED signal thus obtained is given in Fig. 4, plotted as percent difference $\%I_{\mathrm{tot}}(s,t)$,

$$\%I_{\mathrm{tot}}(s,t) = 100 \times \frac{I_{\mathrm{tot}}(s,t) - I_{\mathrm{tot}}(s,0)}{I_{\mathrm{tot}}(s,0)}, \tag{13}$$

where $I_{\mathrm{tot}}(s,t)$ is the signal at time t and $I_{\mathrm{tot}}(s,0)$ is the reference signal at $t = 0$, i.e., the pump-off signal.

To aid in the interpretation in Fig. 4, we have also calculated the static signal, shown in Fig. 5, for all reaction products observed in the AIMC simulations, guided by the reaction pathways in Fig. 3. Representative structures were taken from the trajectories at arbitrary times, showing each reaction observed, and the IAM was then used to calculate the static UED signal for each structure, briefly comprising (a) α-CC bond breaking; (b) β-CC bond breaking; (c) the production of C_2H_4, CH_2, and CO; and also (d) the production of CH_2CO and C_2H_4. The structures for these pathways can be seen in the insets in Fig. 5.

Five key features can be observed in the gas-phase UED of cyclobutanone; these are highlighted by horizontal dashed lines in Fig. 4 at $s = 1.1, 2.2, 4.5, 7.2$, and 9.8 Å^{-1}. Matching these peaks with those observed in Fig. 5, one can see all four reaction products yield a negative feature at ~1.1 Å^{-1} and a positive feature at ~2.2 Å^{-1}, likely making this peak arise from the carbon backbone of cyclobutanone, the breaking of which is common among all reaction pathways. Both features at ~1.1 and ~2.2 Å^{-1} grow in intensity after ~20 fs, matching the timescale shown in Sec. IV A. Both features continue to grow in intensity. Most notably, around 75 fs, Fig. 2 shows that we begin to observe α-CC bond breaking. This, coupled with the high intensity observed in the static signal in Fig. 5(c) at 2.2 Å^{-1}, suggests that the stepwise mechanism to form CO, C_2H_4, and CH_2 requires ~75 fs to form these products. However, we must note that the features in the signal have contributions from all the pathways shown in Fig. 5.

An additional broad positive feature can be observed centered at 4.5 Å^{-1}, with a signal that decays after ~115 fs. Figure 5(c) shows a broad negative feature between the values ~3.75 and ~5.5 Å^{-1}, indicating this reaction pathway causes the depletion of the broad signal. Once again, due to the structural similarities of other reaction pathways, the net signal is a compounded signal with contributions from all products. A similar depletion can be seen in Fig. 5(d). Due to the higher proportion of trajectories being classified as belonging to (d), this likely has a stronger effect on the signal. Depletion of signal in this region is observed in Figs. 5(b)–5(d), having a common feature of β-CC bond breaking, likely making this responsible for the signal depletion.

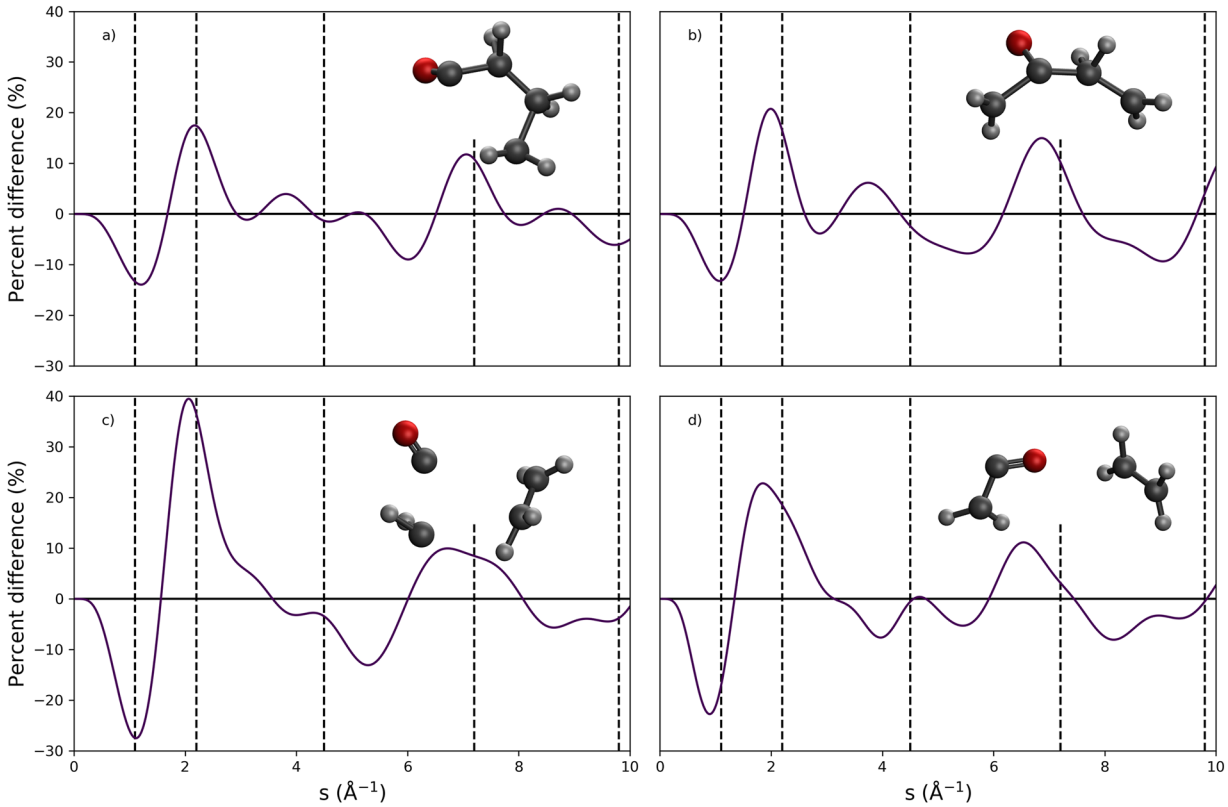

FIG. 5. Static signals obtained for representative structures of pathways observed in AIMC simulations given in percent differences. Panel (a) α-CC ring opening; (b) β-CC ring opening; (c) dissociation to form CO, C_2H_4, and CH_2; and finally (d) CH_2CO and C_2H_4. The structures shown as insets are the geometries from which the static signal is calculated. The five features shown in Fig. 4 are highlighted with vertical dashed lines.

Further peaks can be seen at 7.5 and 9.8 $Å^{-1}$. A peak at 7.5 $Å^{-1}$ can be seen in all pathways with a similar intensity (~10%); therefore, yielding little structural information other than the molecule has moved away from the equilibrium geometry. In contrast, Fig. 5(c) and, to a lesser extent, Fig. 5(d) both show a signal at 9.8 $Å^{-1}$. Thus, it is likely this feature arises from the breaking of the β-CC common to both reaction products.

V. CONCLUSIONS

This work was undertaken in response to the "*Prediction Challenge: Cyclobutanone Photochemistry*" and presents simulated ultrafast electron diffraction (UED) signals for gas-phase cyclobutanone upon photoexcitation into the S_2 electronic state. The main dissociation pathways of photoexcited cyclobutanone were identified with the help of AIMC non-adiabatic dynamics. Then, using these AIMC trajectories, the electronic diffraction was calculated using the IAM method. The calculated UED pattern was compared with static signals for representative structures for the different dissociation pathways observed in the AIMC dynamics. Overall, five key features in the UED pattern can be used to distinguish the reaction channels observed in the AIMC simulation. We find that there is a significant overlap between many features due to a high degree of structural similarity between the different photoproducts, combined with a significant degree of symmetry in cyclobutanone. However, ultimately, we found strong correlations between the timescales and products evident in the simulations and features in the overall UED signal (shown in Fig. 4).

The extent of the work was limited by the strict deadline inherent in the *challenge*, and it is, therefore, straightforward to identify avenues for further work. To begin with, the presented simulations include only the first 200 fs of the cyclobutanone dissociation dynamics, and the degree of sampling, i.e., the number of trajectories propagated, was also limited. Previously, we developed a technique that allowed us to take the pump pulse shape into account and account for the dynamics during the pulse.[48] We have not used this approach here and assumed instant excitation, but it can be straightforwardly done. With longer propagation times, it will also be easy to account for some coupling between coherent states using the so called train basis functions.[35] This approach does not require additional trajectories or electronic structure calculations. It is anticipated to improve the accuracy of the results, although we do not expect qualitative changes since the underlying trajectories remain the same. All of these improvements will be the subject of subsequent work. Longer simulation times will make it possible to make comparisons to the long-term dynamics observed in the experiment, while more trajectories should, in principle, allow us to move beyond the independent and semiclassical trajectory approximation used when calculating the UED signals. In addition, as discussed in the UED theory section, should the experimental data indicate that more subtle effects in the scattering were observed, then *ab initio* simulations of the scattering signal, going beyond the independent atom model, are clearly of interest.

In summary, the present work demonstrates the capability of AIMC to simulate photodynamics in a challenging molecule and that UED signals can be predicted straightforwardly from the simulations. We also note that the AIMC simulations should, in principle, provide a better basis for the prediction of experimental signals that reflect the degree of coherence in the molecule during the dynamics, such as nonlinear spectroscopies or coherent mixed scattering.[64,65]

ACKNOWLEDGMENTS

D.V.M. and D.V.S. acknowledge the support of EPSRC Grant No. EP/P021123/1. Furthermore, D.S., A.K., and D.M. acknowledge the support from EPSRC Programme Grant No. EP/X026973/1. L.H. and A.K. acknowledge the funding from the Leverhulme Trust (Grant No. RPG-2020-208), and A.K. additionally acknowledges EPSRC Grant Nos. EP/V049240/2, EP/V006819/2, and EP/X026698/1. A.K. also acknowledges the support from the Chemical Sciences, Geosciences, and Biosciences Division, Office of Basic Energy Sciences, Office of Science, US Department of Energy, Grant No. DE-SC0020276. This work was carried out using the computational facilities of the Advanced Computing Research Centre, University of Bristol.

AUTHOR DECLARATIONS

Conflict of Interest

The authors have no conflicts to disclose.

Author Contributions

Dmitry V. Makhov: Data curation (equal); Formal analysis (equal); Investigation (equal); Methodology (equal); Resources (equal); Software (equal); Validation (equal); Visualization (equal); Writing – original draft (equal); Writing – review & editing (equal). **Lewis Hutton**: Formal analysis (equal); Investigation (equal); Methodology (equal); Software (equal); Visualization (equal); Writing – review & editing (equal). **Adam Kirrander**: Conceptualization (equal); Data curation (equal); Formal analysis (equal); Funding acquisition (equal); Investigation (equal); Methodology (equal); Project administration (equal); Resources (equal); Software (equal); Supervision (equal); Validation (equal); Visualization (equal); Writing – original draft (equal); Writing – review & editing (equal). **Dmitrii V. Shalashilin**: Conceptualization (equal); Data curation (equal); Formal analysis (equal); Funding acquisition (equal); Investigation (equal); Methodology (equal); Project administration (equal); Resources (equal); Software (equal); Supervision (equal); Validation (equal); Visualization (equal); Writing – original draft (equal); Writing – review & editing (equal).

DATA AVAILABILITY

The data that support the findings of this study are available from the corresponding author upon reasonable request.

REFERENCES

[1] D. Filippetto, P. Musumeci, R. Li, B. Siwick, M. Otto, M. Centurion, and J. Nunes, "Ultrafast electron diffraction: Visualizing dynamic states of matter," Rev. Mod. Phys. **94**, 045004 (2022).

[2] A. A. Ischenko, P. M. Weber, and R. J. D. Miller, "Capturing chemistry in action with electrons: Realization of atomically resolved reaction dynamics," Chem. Rev. **117**, 11066–11124 (2017).

[3] H. Yong, A. Kirrander, and P. M. Weber, "Time-resolved x-ray scattering of excited state structure and dynamics," in *Structural Dynamics with X-Ray*

and Electron Scattering, 1st ed., *Theoretical and Computational Chemistry Series Vol. 25*, edited by K. Amini, A. Rouzée, and M. J. J. Vrakking (Royal Society of Chemistry, United Kingdom, 2024), Chap. 3, p. 344, www.rsc.org.
[4]B. Stankus, H. Yong, J. Ruddock, L. Ma, A. M. Carrascosa, N. Goff, S. Boutet, X. Xu, N. Zotev, A. Kirrander, M. Minitti, and P. M. Weber, "Advances in ultrafast gas-phase x-ray scattering," J. Phys. B: At., Mol. Opt. Phys. **53**, 234004 (2020).
[5]J. Yang, V. Makhija, V. Kumarappan, and M. Centurion, "Reconstruction of three-dimensional molecular structure from diffraction of laser-aligned molecules," Struct. Dyn. **1**, 044101 (2014).
[6]T. Ishikawa, S. A. Hayes, S. Keskin, G. Corthey, M. Hada, K. Pichugin, A. Marx, J. Hirscht, K. Shionuma, K. Onda, Y. Okimoto, S.-y. Koshihara, T. Yamamoto, H. Cui, M. Nomura, Y. Oshima, M. Abdel-Jawad, R. Kato, and R. J. D. Miller, "Direct observation of collective modes coupled to molecular orbital–driven charge transfer," Science **350**, 1501–1505 (2015).
[7]M. Asenov, S. Ramamoorthy, N. Zotev, and A. Kirrander, "Inversion of ultrafast X-ray scattering with dynamics constraints," in *Machine Learning and the Physical Sciences* (NeurIPS, 2020), p. 7.
[8]H. Yong, A. M. Carrascosa, L. Ma, B. Stankus, M. P. Minitti, A. Kirrander, and P. M. Weber, "Determination of excited state molecular structures from time-resolved gas-phase X-ray scattering," Faraday Discuss. **228**, 104–122 (2021).
[9]K. Acheson and A. Kirrander, "Robust inversion of time-resolved data via forward-optimization in a trajectory basis," J. Chem. Theory Comput. **19**, 2721–2734 (2023).
[10]M. H. Beck, A. Jäckle, G. A. Worth, and H. D. Meyer, "The multiconfiguration time-dependent Hartree (MCTDH) method: A highly efficient algorithm for propagating wavepackets," Phys. Rep. **324**, 1–105 (2000).
[11]H. Wang and M. Thoss, "Multilayer formulation of the multiconfiguration time-dependent Hartree theory," J. Chem. Phys. **119**, 1289–1299 (2003).
[12]J. C. Tully, "Molecular dynamics with electronic transitions," J. Chem. Phys. **93**, 1061–1071 (1990).
[13]B. F. E. Curchod and T. J. Martínez, "*Ab initio* nonadiabatic quantum molecular dynamics," Chem. Rev. **118**, 3305–3336 (2018).
[14]T. J. Martinez, M. Ben-Nun, and R. D. Levine, "Multi-electronic-state molecular dynamics: A wave function approach with applications," J. Phys. Chem. **100**, 7884–7895 (1996).
[15]T. J. Martínez and R. D. Levine, "Non-adiabatic molecular dynamics: Split-operator multiple spawning with applications to photodissociation," J. Chem. Soc., Faraday Trans. **93**, 941–947 (1997).
[16]T. J. Martínez, M. Ben-Nun, and R. D. Levine, "Molecular collision dynamics on several electronic states," J. Phys. Chem. A **101**, 6389–6402 (1997).
[17]D. V. Shalashilin, "Quantum mechanics with the basis set guided by Ehrenfest trajectories: Theory and application to spin-boson model," J. Chem. Phys. **130**, 244101 (2009).
[18]K. Saita and D. V. Shalashilin, "On-the-fly *ab initio* molecular dynamics with multiconfigurational Ehrenfest method," J. Chem. Phys. **137**, 22A506 (2012).
[19]S. W. Benson and G. B. Kistiakowsky, "The photochemical decomposition of cyclic ketones," J. Am. Chem. Soc. **64**, 80–86 (1942).
[20]E. K. C. Lee, R. G. Shortridge, and C. F. Rusbult, "Fluorescence excitation study of cyclobutanone, cyclopentanone, and cyclohexanone in the gas phase," J. Am. Chem. Soc. **93**, 1863–1867 (1971).
[21]H. O. Denschlag and E. K. C. Lee, "Benzene photosensitization and direct photolysis of cyclobutanone and cyclobutanone-2-t in the gas phase," J. Am. Chem. Soc. **90**, 3628–3638 (1968).
[22]N. E. Lee and E. K. C. Lee, "Tracer study of photochemically excited cyclobutanone-2-*t* and cyclobutanone. II. Detailed mechanism, energetics, unimolecular decomposition rates, and intermolecular vibrational energy transfer," J. Chem. Phys. **50**, 2094–2107 (1969).
[23]J. C. Hemminger and E. K. C. Lee, "Fluorescence excitation and photodecomposition of the first excited singlet cyclobutanone ($^1A_2$): A study of predissociation of and collisional energy transfer from the vibronically selected species," J. Chem. Phys. **56**, 5284–5295 (1972).
[24]K. Y. Tang and E. K. C. Lee, "Laser photolysis of cyclobutanone. Photodecomposition from selected vibronic levels at long wavelengths," J. Phys. Chem. **80**, 1833–1836 (1976).
[25]E. W. Diau, C. Kötting, and A. H. Zewail, "Femtochemistry of Norrish type-I reactions: II. The anomalous predissociation dynamics of cyclobutanone on the S_1 surface," ChemPhysChem **2**, 294–309 (2001).
[26]M. H. Kao, R. K. Venkatraman, M. N. Ashfold, and A. J. Orr-Ewing, "Effects of ring-strain on the ultrafast photochemistry of cyclic ketones," Chem. Sci. **11**, 1991–2000 (2020).
[27]S. H. Xia, X. Y. Liu, Q. Fang, and G. Cui, "Excited-state ring-opening mechanism of cyclic ketones: A MS-CASPT2//CASSCF study," J. Phys. Chem. A **119**, 3569–3576 (2015).
[28]L. Liu and W. H. Fang, "New insights into photodissociation dynamics of cyclobutanone from the AIMS dynamic simulation," J. Chem. Phys. **144**, 144317 (2016).
[29]C. R. Drury-Lessard and D. C. Moule, "Ring puckering in the $1B2(n, 3s)$ Rydberg electronic state of cyclobutanone," J. Chem. Phys. **68**, 5392–5395 (1978).
[30]L. O'Toole, P. Brint, C. Kosmidis, G. Boulakis, and P. Tsekeris, "Vacuum-ultraviolet absorption spectra of propanone, butanone and the cyclic ketones $C_nH_{2n-2}O$ (n= 4, 5, 6, 7)," J. Chem. Soc., Faraday Trans. **87**, 3343–3351 (1991).
[31]R. F. Whitlock and A. B. Duncan, "Electronic spectrum of cyclobutanone," J. Chem. Phys. **55**, 218–224 (1971).
[32]T. S. Kuhlman, T. I. Sølling, and K. B. Møller, "Coherent motion reveals non-ergodic nature of internal conversion between excited states," ChemPhysChem **13**, 820–827 (2012).
[33]T. S. Kuhlman, S. P. A. Sauer, T. I. Sølling, and K. B. Møller, "Symmetry, vibrational energy redistribution and vibronic coupling: The internal conversion processes of cycloketones," J. Chem. Phys. **137**, 22A522 (2012).
[34]D. V. Makhov, W. J. Glover, T. J. Martinez, and D. V. Shalashilin, "*Ab initio* multiple cloning algorithm for quantum nonadiabatic molecular dynamics," J. Chem. Phys. **141**, 054110 (2014).
[35]D. V. Makhov, C. Symonds, S. Fernandez-Alberti, and D. V. Shalashilin, "*Ab initio* quantum direct dynamics simulations of ultrafast photochemistry with Multiconfigurational Ehrenfest approach," Chem. Phys. **493**, 200–218 (2017).
[36]V. M. Freixas, S. Fernandez-Alberti, D. V. Makhov, S. Tretiak, and D. Shalashilin, "An *ab initio* multiple cloning approach for the simulation of photoinduced dynamics in conjugated molecules," Phys. Chem. Chem. Phys. **20**, 17762–17772 (2018).
[37]D. V. Makhov, K. Saita, T. J. Martinez, and D. V. Shalashilin, "*Ab initio* multiple cloning simulations of pyrrole photodissociation: Tker spectra and velocity map imaging," Phys. Chem. Chem. Phys. **17**, 3316–3325 (2015).
[38]J. A. Green, D. V. Makhov, N. C. Cole-Filipiak, C. Symonds, V. G. Stavros, and D. V. Shalashilin, "Ultrafast photodissociation dynamics of 2-ethylpyrrole: Adding insight to experiment with *ab initio* multiple cloning," Phys. Chem. Chem. Phys. **21**, 3832–3841 (2019).
[39]C. C. Symonds, D. V. Makhov, N. C. Cole-Filipiak, J. A. Green, V. G. Stavros, and D. V. Shalashilin, "Ultrafast photodissociation dynamics of pyrazole, imidazole and their deuterated derivatives using *ab initio* multiple cloning," Phys. Chem. Chem. Phys. **21**, 9987–9995 (2019).
[40]D. V. Makhov and D. V. Shalashilin, "Simulation of the effect of vibrational pre-excitation on the dynamics of pyrrole photo-dissociation," J. Chem. Phys. **154**, 104119 (2021).
[41]D. V. Makhov, S. Adeyemi, M. Cowperthwaite, and D. V. Shalashilin, "Simulation of the dynamics of vibrationally mediated photodissociation for deuterated pyrrole," J. Phys. Commun. **6**, 025001 (2022).
[42]D. V. Shalashilin, "Nonadiabatic dynamics with the help of multiconfigurational Ehrenfest method: Improved theory and fully quantum 24D simulation of pyrazine," J. Chem. Phys. **132**, 244111 (2010).
[43]D. V. Shalashilin, "Multiconfigurational ehrenfest approach to quantum coherent dynamics in large molecular systems," Faraday Discuss. **153**, 105–116 (2011).
[44]D. V. Shalashilin and M. S. Child, "Basis set sampling in the method of coupled coherent states: Coherent state swarms, trains, and pancakes," J. Chem. Phys. **128**, 054102 (2008).
[45]C. Symonds, J. A. Kattirtzi, and D. V. Shalashilin, "The effect of sampling techniques used in the multiconfigurational Ehrenfest method," J. Chem. Phys. **148**, 184113 (2018).

[46]V. M. Freixas, A. J. White, T. Nelson, H. Song, D. V. Makhov, D. Shalashilin, S. Fernandez-Alberti, and S. Tretiak, "Nonadiabatic excited-state molecular dynamics methodologies: Comparison and convergence," J. Phys. Chem. Lett. **12**, 2970–2982 (2021).
[47]V. M. Freixas, W. Malone, X. Li, H. Song, H. Negrin-Yuvero, R. Pérez-Castillo, A. White, T. R. Gibson, D. V. Makhov, D. V. Shalashilin, Y. Zhang, N. Fedik, M. Kulichenko, R. Messerly, L. N. Mohanam, S. Sharifzadeh, A. Bastida, S. Mukamel, S. Fernandez-Alberti, and S. Tretiak, "Nexmd v2.0 software package for nonadiabatic excited state molecular dynamics simulations," J. Chem. Theory Comput. **19**, 5356–5368 (2023).
[48]D. V. Makhov and D. V. Shalashilin, "Floquet Hamiltonian for incorporating electronic excitation by a laser pulse into simulations of non-adiabatic dynamics," Chem. Phys. **515**, 46–51 (2018), part of Special Issue: Ultrafast Photoinduced Processes in Polyatomic Molecules:Electronic Structure, Dynamics and Spectroscopy (Dedicated to Wolfgang Domcke on the Occasion of His 70th Birthday).
[49]A. Moreno Carrascosa, H. Yong, D. L. Crittenden, P. M. Weber, and A. Kirrander, "*Ab initio* calculation of total X-ray scattering from molecules," J. Chem. Theory Comput. **15**, 2836–2846 (2019).
[50]R. M. Parrish and T. J. Martínez, "*Ab initio* computation of rotationally-averaged pump-probe x-ray and electron diffraction signals," J. Chem. Theory Comput. **15**, 1523 (2019).
[51]N. Zotev, A. Moreno Carrascosa, M. Simmermacher, and A. Kirrander, "Excited electronic states in total isotropic scattering from molecules," J. Chem. Theory Comput. **16**, 2594–2605 (2020).
[52]A. M. Carrascosa, J. P. Coe, M. Simmermacher, M. J. Paterson, and A. Kirrander, "Towards high-resolution X-ray scattering as a probe of electron correlation," Phys. Chem. Chem. Phys. **24**, 24542–24552 (2022).
[53]A. Kirrander, K. Saita, and D. V. Shalashilin, "Ultrafast X-ray scattering from molecules," J. Chem. Theory Comput. **12**, 957–967 (2016).
[54]M. Stefanou, K. Saita, D. V. Shalashilin, and A. Kirrander, "Comparison of ultrafast electron and x-ray diffraction – A computational study," Chem. Phys. Lett. **683**, 300–305 (2017).
[55]A. Kirrander and P. M. Weber, "Fundamental limits on spatial resolution in ultrafast X-ray diffraction," Appl. Sci. **7**, 534 (2017).
[56]N. F. Mott and W. L. Bragg, "The scattering of electrons by atoms," Proc. R. Soc. London, Ser. A **127**, 658–665 (1930).
[57]H. Bethe, "Zur Theorie des Durchgangs schneller Korpuskularstrahlen durch Materie," Ann. Phys. **397**, 325–400 (1930).
[58]M. Simmermacher, P. M. Weber, and A. Kirrander, "Theory of time-dependent scattering," in *Structural Dynamics with X-Ray and Electron Scattering*, 1st ed., *Theoretical and Computational Chemistry Series Vol. 25*, edited by K. Amini, A. Rouzée, and M. J. J. Vrakking (Royal Society of Chemistry, United Kingdom, 2023), Chap. 3, p. 85, www.rsc.org.
[59]E. Prince, *International Tables for Crystallography Volume C: Mathematical, Physical and Chemical Tables*, 2006th ed. (Wiley, 2006), ISBN: 978-1-4020-1900-5.
[60]F. Salvat, "Elastic scattering of fast electrons and positrons by atoms," Phys. Rev. A **43**, 578–581 (1991).
[61]F. Salvat, A. Jablonski, and C. J. Powell, "ELSEPA—Dirac partial-wave calculation of elastic scattering of electrons and positrons by atoms, positive ions and molecules," Comput. Phys. Commun. **165**, 157–190 (2005).
[62]P. Debye, "Zerstreuung von Röntgenstrahlen," Ann. Phys. **351**, 809–823 (1915).
[63]H.-J. Werner, P. J. Knowles, F. R. Manby, J. A. Black, K. Doll, A. Heßelmann, D. Kats, A. Köhn, T. Korona, D. A. Kreplin, Q. Ma, T. F. Miller, A. Mitrushchenkov, K. A. Peterson, I. Polyak, G. Rauhut, M. Sibaev, and M. Sibaev, "The Molpro quantum chemistry package," J. Chem. Phys. **152**, 144107 (2020).
[64]M. Simmermacher, A. M. Carrascosa, N. E. Henriksen, K. B. Møller, and A. Kirrander, "Theory of ultrafast x-ray scattering by molecules in the gas phase," J. Chem. Phys. **151**, 174302 (2019).
[65]D. Keefer, F. Aleotti, J. R. Rouxel, F. Segatta, B. Gu, A. Nenov, M. Garavelli, and S. Mukamel, "Imaging conical intersection dynamics during azobenzene photoisomerization by ultrafast x-ray diffraction," Proc. Natl. Acad. Sci. U. S. A. **118**, e2022037118 (2021).